REVIEW ARTICLE OPEN ACCESS

Cooling Of Power Converters by Natural Convection

Saâd Zouitene[1,2,3*], Souad Harmand[1,2], Laurent Remmerie[4], Tewfik Benazzouz[3], Felice Cardarelli[4]
[1]Université Lille Nord de France, F 59000, Lille
[2]UVHC, TEMPO, F-59313 Valenciennes, France
[3]Alstom Transport, Valenciennes, France
[4]Alstom Transport, Charleroi, Belgium

Abstract
This paper discusses the numerical analysis of the effect of a discontinuous heat flux on heat transfer by natural convection along a vertical flat plate or in a rectangular channel. The objective of this study is to determine the effect of a discrete distribution of the heat flux on the cooling of twelve resistors, which represent electronic components, that are mounted on an aluminium vertical plate. The results of the simulations show that the distribution of the heat flux significantly influences the heat transfer.

Nomenclature

Cp	specific heat at constant pressure ($j.kg^{-1}.K^{-1}$)
g	gravitational acceleration ($m.s^{-2}$)
k	thermal conductivity ($W.m^{-1}.K^{-1}$)
P	pressure ($N.m^{-2}$)
e	plate thickness (m)
H	numerical domain height (m)
h	plate (channel) height (m)
d	channel width (m)
T	temperature (K)
u	horizontal velocity component ($m.s^{-1}$)
v	vertical velocity component ($m.s^{-1}$)
x, y	space coordinates (m)
Dimensionless numbers	
Nu	Nusselt number
Nu_y	local Nusselt number
Pr	Prandtl number
Ra	Rayleigh number
x*	dimensionless horizontal coordinate
y*	dimensionless vertical coordinate
Greeks symbols	
β	thermal expansion coefficient (K^{-1})
λ	thermal conductivity ($kg.m^{-1}.K^{-1}$)
μ	dynamic viscosity ($kg.m^{-1}.s^{-1}$)
ρ	density ($kg.m^{-3}$)
φ	heat flux ($W.m^{-2}$)
Subscripts	
s	solid
g	gas
in	inlet
out	outlet
w	wall
∞	ambient condition
c	convective

I. Introduction

Natural convection in a channel or along a vertical flat plate has been the focus of extensive investigations for many years, due to its frequent use in industry and in engineering applications, such as in electronic component cooling, food processing, the chemical and metallurgical industries, nuclear reactor design and passive solar heating.

There have been several numerical **[1,2]** and experimental **[3-5]** investigations on the natural convection in channels that is driven by a temperature difference along the vertical walls. However, the channel geometry and the thermal boundary conditions strongly influence this natural convection.

In reference **[6]** authors analysed the effect of heterogeneous wall temperatures on a vertical flat plate. The authors showed that the buoyancy forces are locally affected by the slope of the temperature profile and that the heat transfer is strongly influenced by the wall temperature distribution.

Reference **[7]** presents a numerical study of natural convection in an obstructed vertical channel with an aspect ratio of 5 and with two symmetric isothermal or adiabatic ribs. The obtained results showed that, for high Rayleigh values, the mean Nusselt number could be increased by increasing the distance of the ribs from the inlet and by moving the ribs towards the outlet. The authors also found that the inlet flow rate always decreased when the distance of the obstruction from the leading edge of the channel was increased for any channel Rayleigh number.

Authors **[8]** studied numerically analysed natural convection enhancement in a vertical, rectangular cross-section channel. The authors found that the mass flow rate varied proportionally to the Grashof

number based on the heated plate height and the heated channel aspect ratio. The authors also found that the maximum wall temperature decreased with increasing aspect ratio and Grashof number.

In reference **[9]** authors investigated experimentally and numerically turbulent natural convection in a vertical, rectangular cross-section channel. The authors obtained the velocity and the turbulent kinetic energy profiles for five configurations at five different vertical positions along the channel. Their results showed that a fully turbulent flow was obtained near the outlet. The authors also noted that the value and distribution of the turbulent kinetic energy at the inlet considerably affected the predicted heat transfer and induced flow rate.

Theoretical and numerical studies of the two-dimensional conjugate free convection that was due to a vertical plate adjacent to a semi-infinite fluid region are presented in reference **[10]**. The authors studied the effects of the finite aspect ratio of the heated plate and concluded that, for a large Rayleigh number, the deviation in the temperature at the fluid/solid interface from the average temperature was less for larger aspect ratios than for smaller ones.

Authors **[11]** investigated numerically natural convection in an air-filled enclosure with a non-uniform heat source mounted centrally on the bottom wall. The authors found that, for $Gr = 10^6$, a non-uniform heating of the heat source significantly enhanced the overall heat transfer rate compared with the rate from a uniform heating of the heat source, whereas this effect was marginal for $Gr = 10^7$.

[12] experimentally and numerically investigated natural convection from a vertical, electrically heated plate that was symmetrically placed in a chimney of variable height. The authors analysed the temperature distribution dependence on the flow field and found that the air flow rate on the heating plate and the overall mass flow rate through the chimney increased with increasing chimney height.

[13] presented a method for determining the optimal distribution and sizes of discrete heat sources in a vertical open channel that is cooled by natural convection. The authors considered two types of geometries: (i) heat sources with a fixed size and a fixed heat flux and (ii) a single heat source with a variable size and a fixed total heat. Their objective was to minimise the temperature of a hot spot that occurred at a point on the wall. The authors numerically showed that the spacing between the discrete heat sources with a fixed size and a fixed heat flux that are attached to an open channel with natural convection can be optimised for maximal global thermal conductance.

In this study, we analyse and optimise the cooling of the electronic components of a train (figure 1). The effect of the electronic components is represented by a discontinuous distribution of the heat flux. We also analyse the effect of the rectangular section of the channel to determine how the train walls influence the heat transfer.

The purpose of this industrial project is to reduce the economic and environmental impact of auxiliary power converters on railway transport. Auxiliary power converters are used to supply air conditioners, emergency devices, batteries and (electric) lighting. Currently, these converters are placed under the floor or on the roof of trains and are cooled by forced convection using fans. The purpose of this project is to reduce the bulk, weight and energy consumption of these converters. A reduction in the size and weight of the converters can be achieved by using high switching frequency components, which enables the placing of the converters inside the trains (figure 1). Once placed in the lateral walls of the train, the converters can be cooled by natural convection. In this work, we study the efficiency of the cooling of the converters by natural convection. We chose to study the case of the train at the stop position which we consider as critical case. We thus chose to study the case of the train at the stop position which we consider as critical case. During running, the condition in the entrance of the channel is an imposed speed which allows improving the cooling obtained by natural convection.

II. Modelling

In this work, natural convection in a two-dimensional channel with length h and width d is considered. The purpose of the present study is to determine the influences of the heat flux distribution (figure 2) and of the channel dimensions on the efficiency of the cooling by natural convection.

The geometry and coordinate system of the present problem are shown in figure 3. The directions of the velocity components u and v are also shown. Three positions were chosen based on the distribution of the imposed heat flux on the vertical plate.

The natural convection fluid flow and heat transfer along the vertical plate that were considered in this study were simulated using the software "Comsol Multiphysics".

The third direction of the plate, which is perpendicular to the plane of the diagram, is assumed to be long enough that the problem can be considered two-dimensional.

1.1. Mathematical formulation

The physical properties of the aluminium plate and of air are assumed to be homogeneous and independent of temperature in the range that was studied, except for the density of the air, which is considered to be a linear function of temperature (the Boussinesq hypothesis).

$$r_g = r_{g¥}\left[1 - b_T\left(T - T_¥\right)\right] \quad (1)$$

The flow along the vertical plate is entirely induced by buoyancy. Air near the plate is initially at the ambient conditions T_∞ and ρ_∞. Thermal radiation is neglected. The plate has a constant discontinuous heat flux φ that is imposed on its external surface.

In the present formulation, the energy equations are written for the steady state for each domain, and useful boundary conditions are provided. We obtain the following equations:

In the solid

We assume that the conductivity of the heated plate is homogeneous and independent of temperature. Thus, the energy equation in the solid medium is:

$$\frac{\partial^2 T}{\partial x^2} + \frac{\partial^2 T}{\partial y^2} = 0 \quad (2)$$

In the gas

The flow is considered two-dimensional and is laminar, and the Boussinesq hypothesis is used. Moreover, we assume that the radiative heat transfer and the viscous dissipation are negligible. Thus, the conservation equations are:

$$\frac{\partial u}{\partial x} + \frac{\partial v}{\partial y} = 0 \quad (3)$$

$$r_g\left(u\frac{\partial u}{\partial x} + v\frac{\partial u}{\partial y}\right) = -\frac{\partial p}{\partial x} + m_g\left(\frac{\partial^2 u}{\partial x^2} + \frac{\partial^2 u}{\partial y^2}\right) \quad (4)$$

$$r_{g¥}\left(u\frac{\partial v}{\partial x} + v\frac{\partial v}{\partial y}\right) = -\frac{\partial p}{\partial y} + m_g\left(\frac{\partial^2 v}{\partial x^2} + \frac{\partial^2 v}{\partial y^2}\right) + gr_{g¥}\left[b_T\left(T - T_¥\right)\right] \quad (5)$$

$$u\frac{\partial T}{\partial x} + v\frac{\partial T}{\partial y} = \frac{l_g}{r_g Cp_g}\left(\frac{\partial^2 T}{\partial x^2} + \frac{\partial^2 T}{\partial y^2}\right) \quad (6)$$

Eq. (3) represents the overall mass balance in a differential volume at a fixed location. Eqs. (4) and (5) represent Newton's second law of motion for Newtonian fluids. Eq. (6) is the first law of thermodynamics applied to a differential volume of fluid.

1.2. Boundary conditions

The hydrodynamic boundary conditions that were used in this work are:

$$u = v = 0 \text{ at } x = 0 \text{ and } x = L \text{ and } -h1 \le y \le H - h1 \quad (7)$$

$$u = v = 0 \text{ at } y = -h1 \text{ and } 0 \le x \le L \quad (8)$$

$$p_{y=H-h1} = P_¥ \quad (9)$$

Eqs. (7) and (8) assume non-slip conditions at the solid domain and at the Plexiglas walls.

The thermal boundary conditions were set as follows. The heat fluxes that were applied to the aluminium plate are constant and discontinuous:

$$-l_s\left(\frac{\partial T}{\partial x}\right)_{x=-e} = j\,f(y) \quad (10)$$

$$f(y) = \begin{cases} 1 & \text{if } 0.15 \le y \le 0.25;\ 0.35 \le y \le 0.45;\ 0.55 \le y \le 0.65;\ 0.75 \le y \le 0.85. \\ 0 & \text{else} \end{cases}$$

$$-l_s\left(\frac{\partial T}{\partial y}\right)_{y=0} = -l_s\left(\frac{\partial T}{\partial y}\right)_{y=h} = 0 \quad (11)$$

The continuity condition (Eq. (12))

$$-l_s\left(\frac{\partial T}{\partial x}\right)_{x=0,0\le y\le h} = -l_g\left(\frac{\partial T}{\partial x}\right)_{x=0,0\le y\le h} \quad (12)$$

1.3. Numerical model

The numerical domain (figure 3) is composed of an extension that is upstream of the inlet (1), the main channel (2), an extension that is downstream of the outlet (3) and an extension for air recirculation (4). We use this domain decomposition to eliminate the need to specify inaccurate velocity and temperature profiles at the entrance and exit of the channels, which enables us to have only the effect of natural convection in the numerical simulation. Velocity and temperature profiles are imposed on the extremes of

the domain. The dimensions of the (1), (3) and (4) extensions were selected to ensure that these extensions do not influence the variations in the maximal temperature for the configurations that were simulated. We compared the variations in the maximal temperature for different dimensions of the extensions; we varied the lengths of extensions (1) and (3) and the width of extension (4). The tests showed that the solution becomes relatively insensitive to these dimensions when the length of extension (1) is > h and when the width of extension (4) is > 25d.

III. Experimental setup

An experimental facility has been constructed for performing natural convection tests, with the main emphasis on heat transfer phenomena. The facility's characteristics were suitable for studies of the chimney effect. **Figure X** shows an outline of the experimental arrangement. The apparatus consists mainly of the following components:

Aluminium Plate

The aluminium plate was 500 mm wide, 1000 mm long and 12 mm thick, with a thermal conductivity of 237 $W{\cdot}m^{-1}{\cdot}K^{-1}$. The coefficient of thermal expansion was not taken into account.

Power Supply & Heat system

The power supply provided a variable DC output. The model selected was the Sorensen/Ametek XFR 150-18, which has a voltage range of 0–150 V and a current range of 0–18 A. The power supply provided energy to twelve resistors that were placed uniformly in three columns and four rows. The resistors are used to simulate the heat flux produced by the electrical converters inside the train. The imposed heat flux was varied between 1600 and 3200 $W{\cdot}m^{-2}$. Each resistor had a resistance of approximately 0.8 Ohm and supported a maximum current of 15.8 A. As consequence, each resistor could support a maximum of 200 W with an uncertainty ọf±10 $W{\cdot}m^{-2}$.

Insulation

To guarantee that the totality of the imposed heat flux was used to heat the aluminium plate, fibreglass was placed around the resistors. The thermal conductivity of the fibreglass was 0.04 $W{\cdot}m^{-1}{\cdot}K^{-1}$, so it acted to insulate the resistors. Negligible losses were assumed.

Thermocouples

To measure the temperature of the plate, forty K-thermocouples were used, each with an uncertainty $\Delta T=\pm 0.05$ °C. The distribution of the thermocouples is shown in figures 5.c and 5.d.

Acquisition data system

To measure temperatures, a data acquisition data system was used. The system was the Keithley 3700, which can measure up to 80 different channels. This machine allows the user to vary the number of measurements and the time interval between measurements. The Keithley 3700 was connected to a computer to record all temperatures.

Thermo-Anemometer

A Kimo VT100 thermo-anemometer was used to measure the velocity of the air and its temperature. The velocity range was from 0.15 m/s to 10 m/s, and the temperature range was from -20 ºC to 80 ºC. The maximum uncertainty was 0.2 m/s in the velocity and 0.25 ºC in the temperature.

The experimental procedure was as follows:

- A heat density flux is imposed by fixing the voltage and the current delivered by the generator.
- The aluminium plate temperatures and the ambient temperature are recorded.
- The air speed at the top of the plate is recorded.

3.1. Direct method

The direct model involves solving partial differential equations related to the cooling of the plate. This model allows the local plate's temperature $T_{cal}(x,y)$ to be computed**.** The 2D equation in the direct model is:

$$p(x,y)+\lambda\left(\frac{\partial^2 T_w(x,y)}{\partial x^2}+\frac{\partial^2 T_w(x,y)}{\partial y^2}\right)=\frac{1}{e}\varphi_w(x,y) \quad (1)$$

where p(x,y) is the volumetric electrical dissipated heat flux and $\varphi_w(x,y)$ is the local wall heat flux. The boundary conditions on the plate (i.e., $T_w(0,y)$, $T_w(H,y)$, $T_w(x,0)$, $T_w(x,L)$, $0\le H\le 1$ m, $0\le L\le 0.5$ m) are given by the experimental measurements. To solve the direct model, the distribution of the heat flux $\varphi_w(x,y)$ is assumed to be known. Equation (1) is discretised and then solved by finite differences with an implicit scheme using central differences for second-order terms. The finite-difference scheme is then:

$$p_j^i+\lambda\left(\frac{T_j^{i+1}-2T_j^i+T_j^{i-1}}{\Delta x^2}+\frac{T_{j+1}^i-2T_j^i+T_{j-1}^i}{\Delta y^2}\right)=\frac{1}{e}\left[\varphi_{wj}^{\ i}\right] \quad (2)$$

with

$$1\le i\le M,\ 1\le j\le N \quad \text{and} \quad \Delta x=\frac{L}{M+1},\ \Delta y=\frac{H}{N+1}$$

Equation (2), written using a matrix A of dimensions (M)×(N-1), allows the calculation of the temperature matrix:

$$[p]+[A].[T]=\frac{1}{e}[\varphi]$$

$$[T_{cal}]=\frac{1}{e}.[A]^{-1}.[\varphi]-[p] \quad (3)$$

3.2. Inverse method

The inverse method allows the distribution $\varphi_w(x,y)$ to be determined by comparing the computed and the measured temperature evolutions during the cooling process. To reduce the effect of measurement noise on the parameter to be identified, we use a spatial regularisation. As explained by Tikhonov et al. [20], this model involves searching for the distribution $\varphi_w(x,y)$ that will minimise the following function:

$$S=\sum_x\sum_y\left[T_{cal}(x,y)-T_{mes}(x,y)\right]^2+\alpha\sum_x\sum_y\left[grad(\varphi_w(x,y))\right]^2 \quad (4)$$

During the iterative process, the local wall flux $\varphi_w^{k+1}(i,j)$ at iteration k+1 is determined knowing the flux $\varphi_w^{k}(i,j)$ at iteration k and that it minimises the function S in equation (4):

$$\varphi_w^{k+1}(i,j)=\varphi_w^{k}(i,j)+\Delta\varphi_w^{k}(i,j) \quad (5)$$

$$\Delta\varphi_w^{k}(i,j)=-\left\{[J][J]^t+\alpha[X]\right\}^{-1}\left\{[J]\left(\left[T_{cal}^{k}\right]\left[\varphi_w^{k}\right]-[T_{mes}]+\alpha[X]\left[\varphi_w^{k}\right]\right)\right\} \quad (6)$$

$$[J]=\left[\frac{\partial T_{cal}^{k}\left(\varphi_w^{k+1}\right)}{\partial\varphi_w^{k+1}}\right] \text{ and } [X]=\frac{1}{2}\left[\frac{\partial S_1}{\partial\varphi_w^{k+1}}\right]\left[\varphi_w^{k+1}\right]^{-1}$$

The regularisation parameter is used to minimise the effect of the measurement noise on the identified local wall heat flux. The optimal values of correspond to the optimum of the matrix $\left([J][J]^t+\alpha[X]\right)$ conditioning.

$$\text{cond}\left([J][J]^t+\alpha^{opt}[X]\right)=\min\left\{\text{cond}\left([J][J]^t+\alpha[X]\right)\right\} \quad (7)$$

The iterative process is stopped when two successive matrices of the calculated temperatures do not differ significantly.

IV. Results and Discussion

4.1. Model validation

4.1.1. Comparison with the bibliography

The calculations were conducted using the commercial code Comsol Multiphysics 4.2.

The numerical code was validated using the numerical results of Desrayaud and Lauriat **[13]**. These authors studied the mixed convection of air in a vertical parallel plate channel and obtained the dimensionless axial velocity (figure 4.a) and temperature profiles (figure 4.b) for Re = 300 and Gr = $1.59.10^5$.

As shown in this figure, the simulations results of **[14]** are in good agreement with our present work.

4.1.2. Comparison with experimental results

A model of configuration position B was used to compare numerical and experimental results. For this comparison, we used a power of 200 W and the ambient temperature was approximately 20°C. To obtain the steady state, the experimental test lasted for a little more than 7 hours. Figure 6 shows that the numerical and experimental results for the plate temperature are very close. The maximum error does not exceed 5 %.

4.2. Effect of the heat flux distribution

We numerically studied the effect of the heat flux distribution on the heat transfer over a free plate (without a channel). We compare the results for the three configurations A, B and C, which depend on the positions of the components on the plate (figure 2). For this numerical study, the ambient temperature is set to 20°C and the total imposed power is set to 200 W.

4.2.1. Wall temperature

The temperature profiles of the heated plate for the three configurations are shown in figure 7. We observe a temperature peak for the two positions A and C, in contrast with position B, for which the profiles remain constant over most of the plate. The temperature reaches its maximum in the areas where the components are installed. Position C provides a better heat transfer. A maximum temperature is reached for position A.

Natural convection cooling is influenced by the distribution of the discrete heat flow on the plate; it is more efficient when all of the components are placed at the bottom of the plate.

4.2.2. Local Nusselt number

For the case of a free vertical flat plate and for each configuration, the local Nusselt number was compared with different data from the bibliography for laminar and turbulent flows with a constant heat flux and a constant temperature. In the case of a plate

at constant temperature, we use the data of Mc Adams **[15]** and **[16]:**

Nu_y	*Laminar*	*Turbulent*
Constant T°	$0.39\ Re^{1/4}$ **[15]**	$0.12\ Ra^{1/3}$ **[15]**
Constant heat flux	$\frac{0.670 Ra^{*1/4}}{\left(0.437 / Pr\right)^{4/9}}$ **[16]**	$0.13\ Ra^{*1/3}$ **[15]**

To calculate the local Nusselt number from our numerical results, we use the following expression:

$$Nu_y = \frac{j_c y}{l\,(T_w - T_\infty)} \qquad (13)$$

The local Nusselt number and the chosen numerical data are presented in figure 8 for the three configurations. None of the studied data correspond to the results that were numerically obtained for the three configurations. This result proves that the distribution of the discrete heat flux strongly influences the convective heat transfer. Figure 9 shows the local Nusselt number profiles for the three configurations. The results are consistent with the temperature results. The Nusselt number is better at the top of the vertical plate for position C, which indicates a better heat exchange and thus better cooling.

4.2.3. Air temperature

Figure 10 shows the variations in the air temperature at different positions on the plate: y = 0.05 m, y = 0.5 m and y = 0.95 m. The temperature profiles are monotonic. The gradient of the air temperature is large near the heated wall and becomes relatively small away from the wall. For configuration C, the air temperature is higher near the lower part of the plate. Close to the top of the plate, the air temperature is more significant for the two configurations A and B.

4.2.4. Air velocity profiles

To quantify the effect of the heat flux distribution on the air velocity, figure 11 shows the vertical air velocity profiles at several positions on the plate: y = 0.05 m, y = 0.5 m and y = 0.95 m. For the three configurations and at all of the positions, the air vertical velocity is large near the heated plate. This result can be explained by the effect of natural convection. The higher the vertical position on the plate, the higher the magnitude of the vertical velocity. The density of the hot air that is in contact with the heated plate is less than the density of cold air. Therefore, warm air rises to the top and the magnitude of the air velocity increases. The magnitude of the air velocity for configuration C is more significant along the plate, which is consistent with the results that were obtained for the plate temperature profiles. This configuration enables a better heat transfer.

4.3. Effect of the channel dimension

4.3.1. Wall temperature

We added an insulating, vertical wall parallel to the heated plate to form a channel to study the effect of the distance *d* between the two plates (the channel width). Figure 12 shows the temperature profiles along the vertical plate for channel widths of d = 5 cm and d = 10 cm and for the free vertical plate. The presence of the insulating plate at d = 10 cm improves the heat transfer at the bottom of the heated plate and slightly degrades the efficiency of the cooling at the top.

The distance between the two plates significantly influences the heat transfer. We note that the temperature reaches a maximum for the three configurations for d = 5 cm. A reduction in the size of the channel significantly degrades the cooling efficiency.

Figure 13 shows a comparison of the temperature profiles for each configuration when d = 5 cm and d = 10 cm. The results are similar to those discussed in section 3.2. The temperature slowly increases through the plate for configuration B. We also notice temperature peaks for the two positions A and C. Position C provides a better cooling at the top of the plate, while configuration A provides a better cooling at the bottom. We reach a maximum temperature for position A.

4.3.2. Air temperature

Figure 14 shows the air temperature profiles in the channel for two cases: channel widths of d = 5 cm and d = 10 cm. The temperature is monotonic at the entrance of the channel for the two cases. At the exit of the channel, the temperature is almost constant. The temperature is more constant at the exit for the channel with the smaller width. The size of this channel is too small; therefore, the evacuation of warm air is not efficient enough. The magnitude of the temperature is significantly larger for the channel with a smaller width. At the entrance of the two channels, the temperature profiles are almost identical.

4.3.3. Air velocity profiles

Natural convection flow along a vertical channel is expected to be laminar at the inlet in the absence of any disturbances and to become turbulent near the outlet depending on the geometric size of the channel and the thermal parameters. Figure 15 shows the profiles of the vertical air velocity at the entrance and exit of the two channel with widths of d = 5 cm and d = 10 cm. The numerical vertical velocity profiles

indicate that the velocity peak becomes more significant as we approach the channel exit. We note that the magnitude of the velocity is higher when the channel width is d = 10 cm than when it is d = 5 cm, which explains the difference in the heated plate temperatures between the two channels (figure 14). For the case of d = 10 cm, we have a better acceleration of the air particles near the heated wall; thus, the thermal boundary layer is smaller, which enables a better cooling

V. Conclusions

The discrete distribution of the heat flux influences the heat transfer. A better heat transfer is obtained by placing all of the components at the bottom of the plate.

The width of the channel significantly changes the results that were obtained for the temperature profiles along the plate; for d = 5 cm, we reach a very high temperature compared with that for d = 10 cm. These results can be explained by analysing the vertical velocity; its magnitude is more significant for the larger channel and enables a better heat transfer.

Configuration C ensures a better cooling at the bottom of the heated plate, while configuration B ensures a better cooling at the top of the plate. Configuration A is not useful for cooling the electronic components in our study; we reach a notably high temperature at the component positions, which can damage the components.

References

[1] M.E. Newell, F.W. Schmidt, Heat transfer by laminar natural convection within rectangular enclosures, J. Heat Transfer 92 (1970) 159-168.

[2] J.E. Drummond, S.A. Korpela, Natural convection in a shallow cavity, J. Fluid Mech. 182 (1987) 543–564.

[3] S.H. Yin, T.Y. Wung, K. Chen, Natural convection in an air layer enclosed within rectangular cavities, Int. J. Heat Mass Transfer 21 (1978) 307-315.

[4] S. Tian, T.G. Karayiannis, Low turbulence natural convection in an air filled square cavity. Part I: the thermal and fluid flow fields, Int. J. Heat Mass Transfer 43 (2000) 849-866.

[5] N. Seki, S. Fukusako, H. Inaba, Visual observation of natural convection flow in a narrow vertical cavity, J. Fluid Mech. 84 (1978) 695–704. ,

[6] M. Havet, D. Bay, Natural convection over a non-isothermal vertical plate, Int. J. Heat Mass Transfer 42 (1999) 3103-3112

[7] G. Desrayaud, A. Fichera, Laminar natural convection in a vertical isothermal channel with symmetric surface-mounted rectangular ribs, Intl. J. Heat and Fluid Flow 23 (2002) 519-529.

[8] A. Andreozzi, A. Campo, O. Manca, Compounded natural convection enhancement in vertical parallel-plate channels, Intl. J. Thermal Sciences 47 (2008) 742–748.

[9] T. Yilmaz , S. M. Fraser, Turbulent natural convection in a vertical parallel-plate channel with asymmetric heating, Intl. J. Heat and Mass Transfer 50 (2007) 2612–2623. ,

[10] M. Vynnycky and S. Kimura,Conjugate free convection due to a heated vertical plate, Int J. Heat Mass Transfer. Vol 39, No 5, pp 1067-1080, 1996.

[11] S. Saravanan, C. Sivaraj, Natural convection in an enclosure with a localized nonuniform heat source on the bottom wall, Int.l J.Heat Mass Transfer 54 (2011) 2820-2828

[12] S.Kazansky and V.Dubovsky, Chimney-enhanced natural convection from a vertical plate: experiments and numerical simulations, Int J. Heat Mass Transfer. Vol 46, pp 497-512, January 2003

[13] A.Silva and G.Lorenzini, Distribution of heat sources in vertical open channels with natural convection, Int J. Heat Mass Transfer. Vol 48, pp 1462-1469, 2005

[14] G. Desrayaud and G. Lauriat,Flow reversal of laminar mixed convection in the entry region of symmetrically heated, vertical plate channels, Int J. Thermal Sciences. 48 (2009) 2036-2045.

[15] Mc Adams (W.H.). – Transmission de la chaleur. Dunod (1961)

[16] Petit (J.P.). – Convection naturelle. Cours ECP

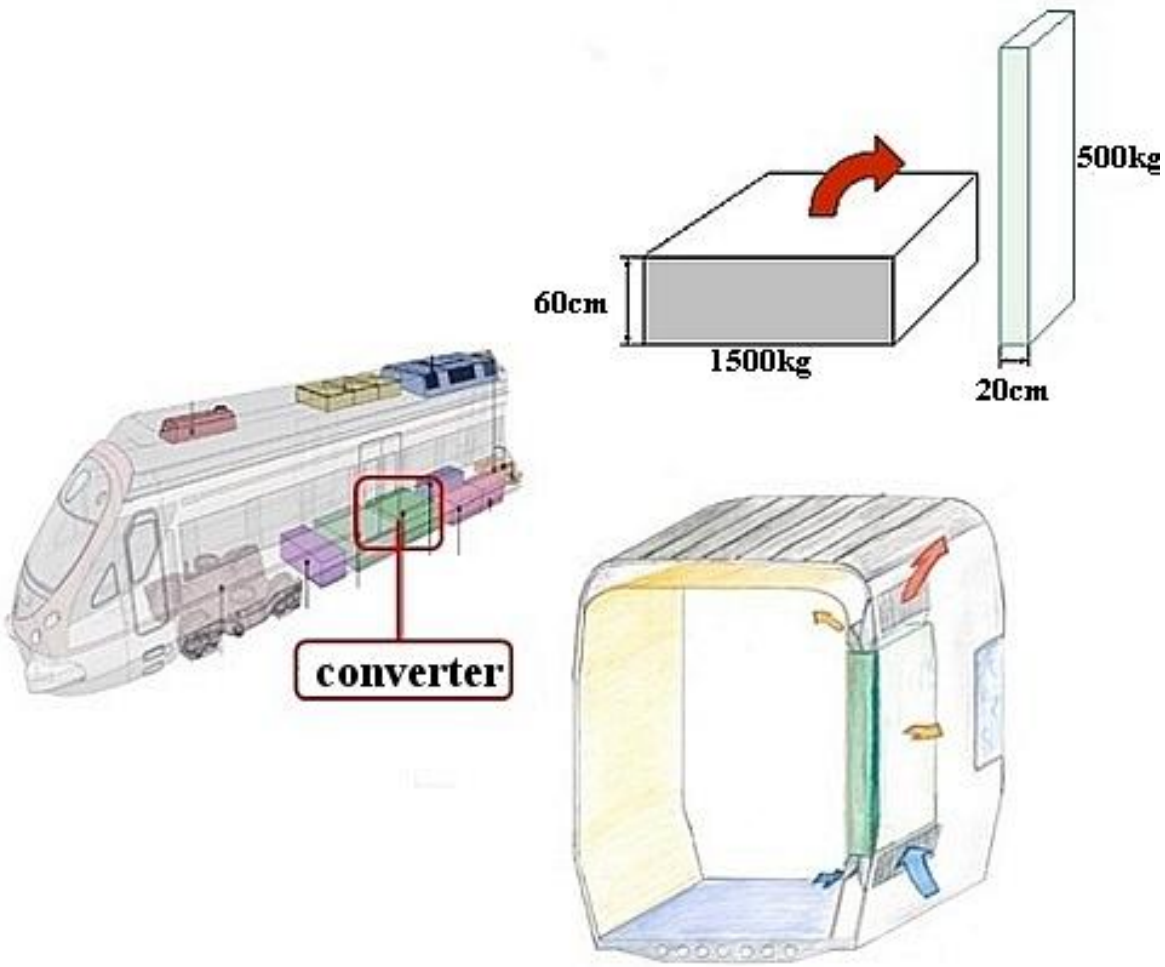

Figure 1 : Description of the electronic component on the train

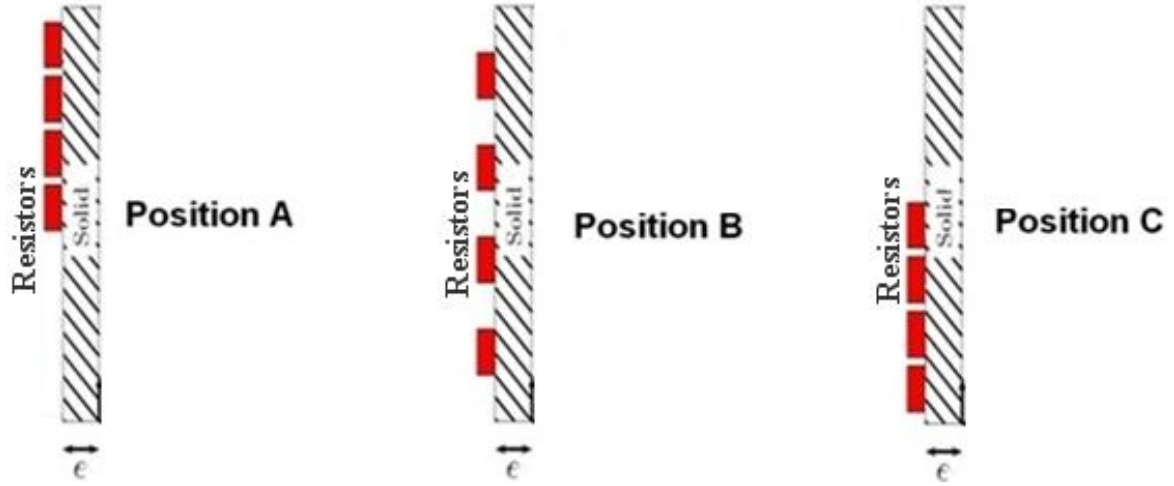

Figure 2 : the three configurations chosen for the study

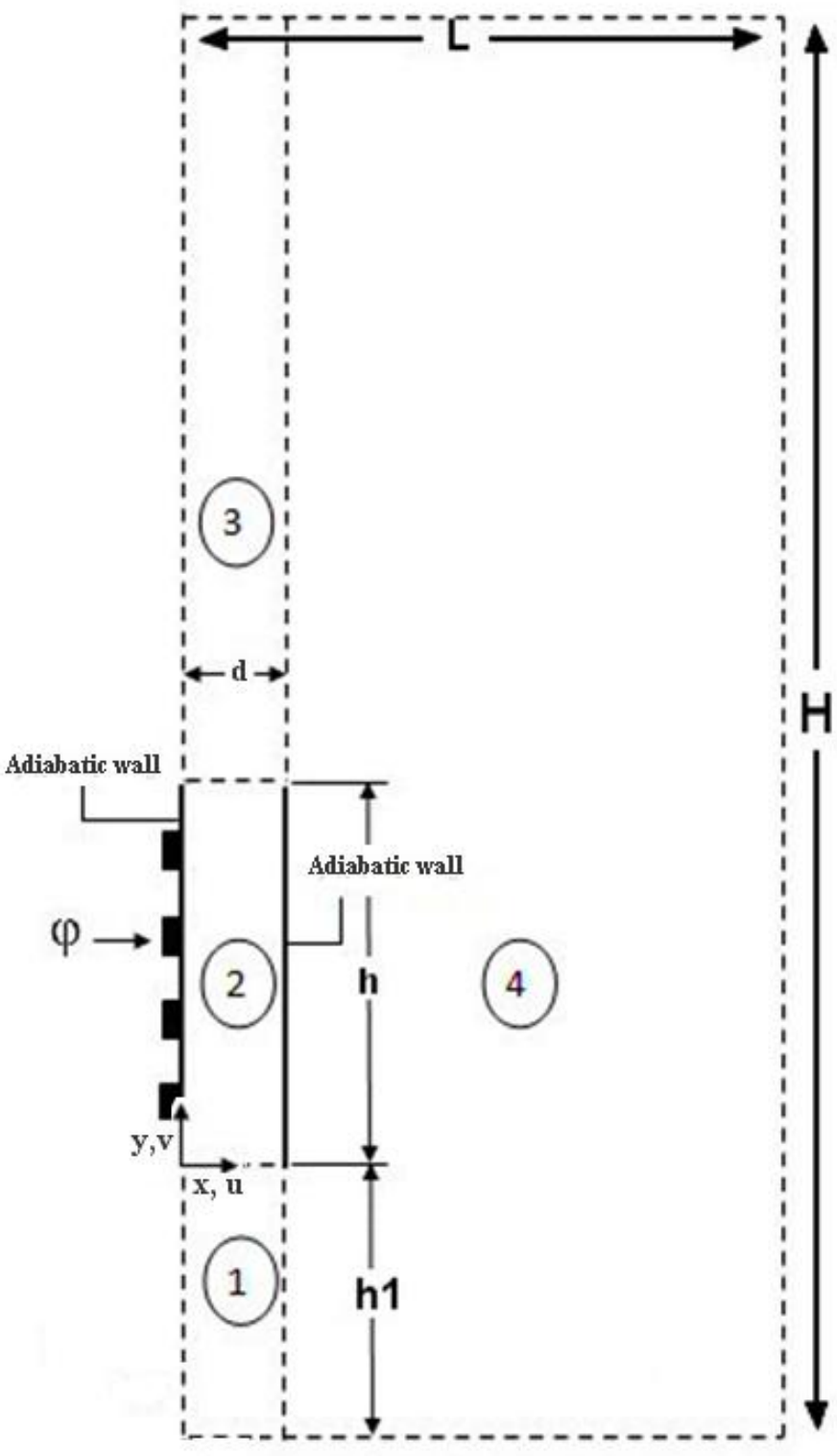

Figure 3 : Geometry and numerical domain

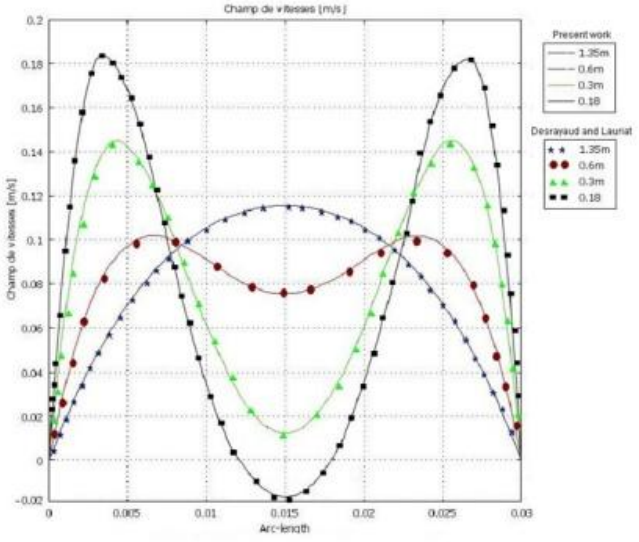

(a)

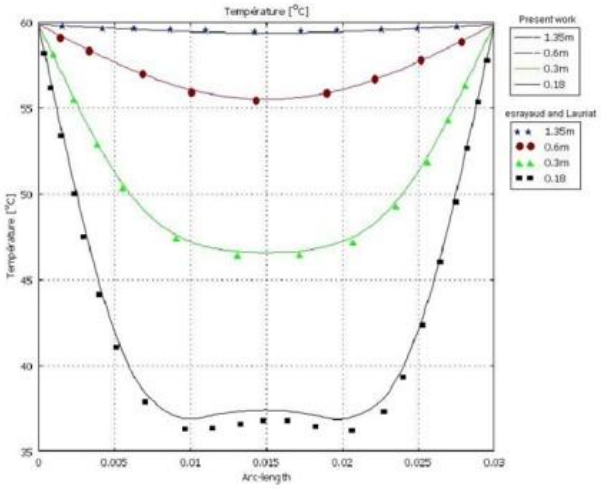

(b)

*Figure 4 : Numerical validation of the study **(a)** Comparison of our air velocity profiles and [14] velocity profiles **(b)** comparison of our air temperature profiles and [14] velocity profiles*

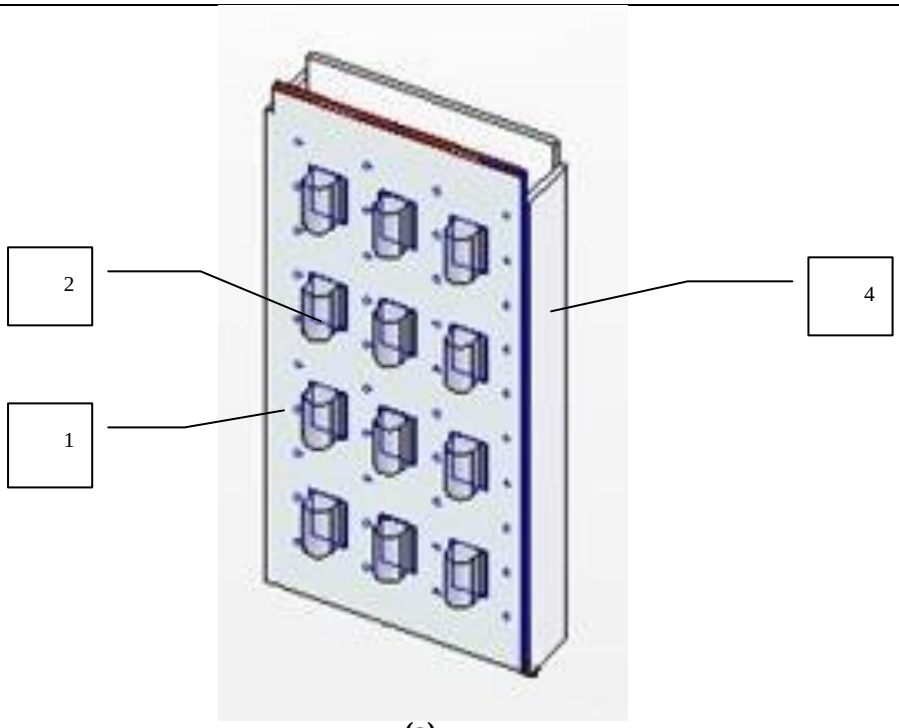

(a)

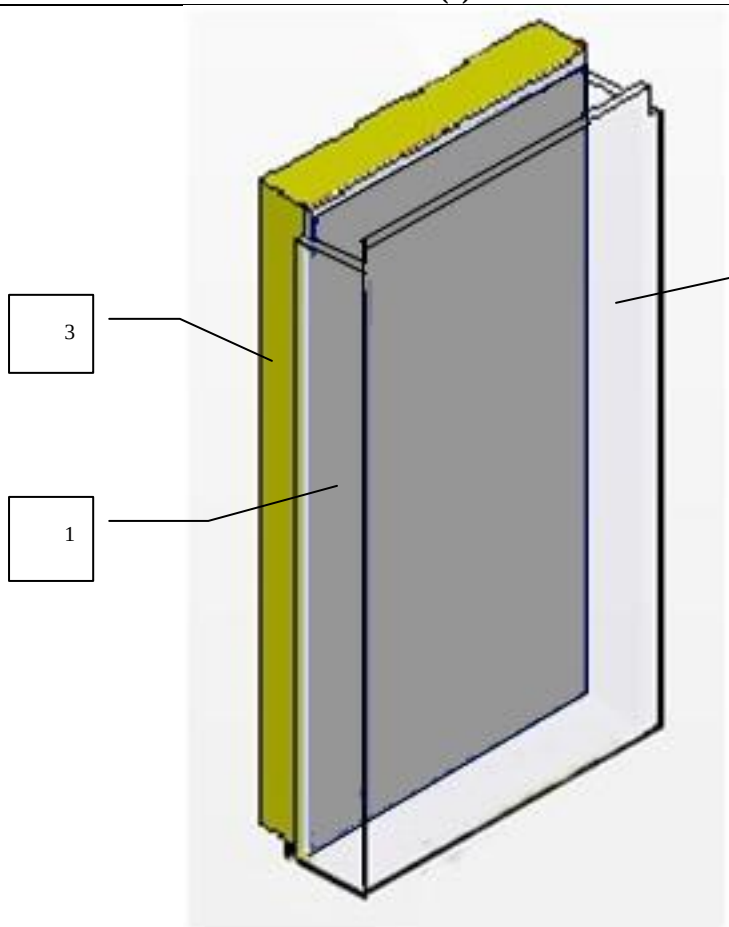

(b)

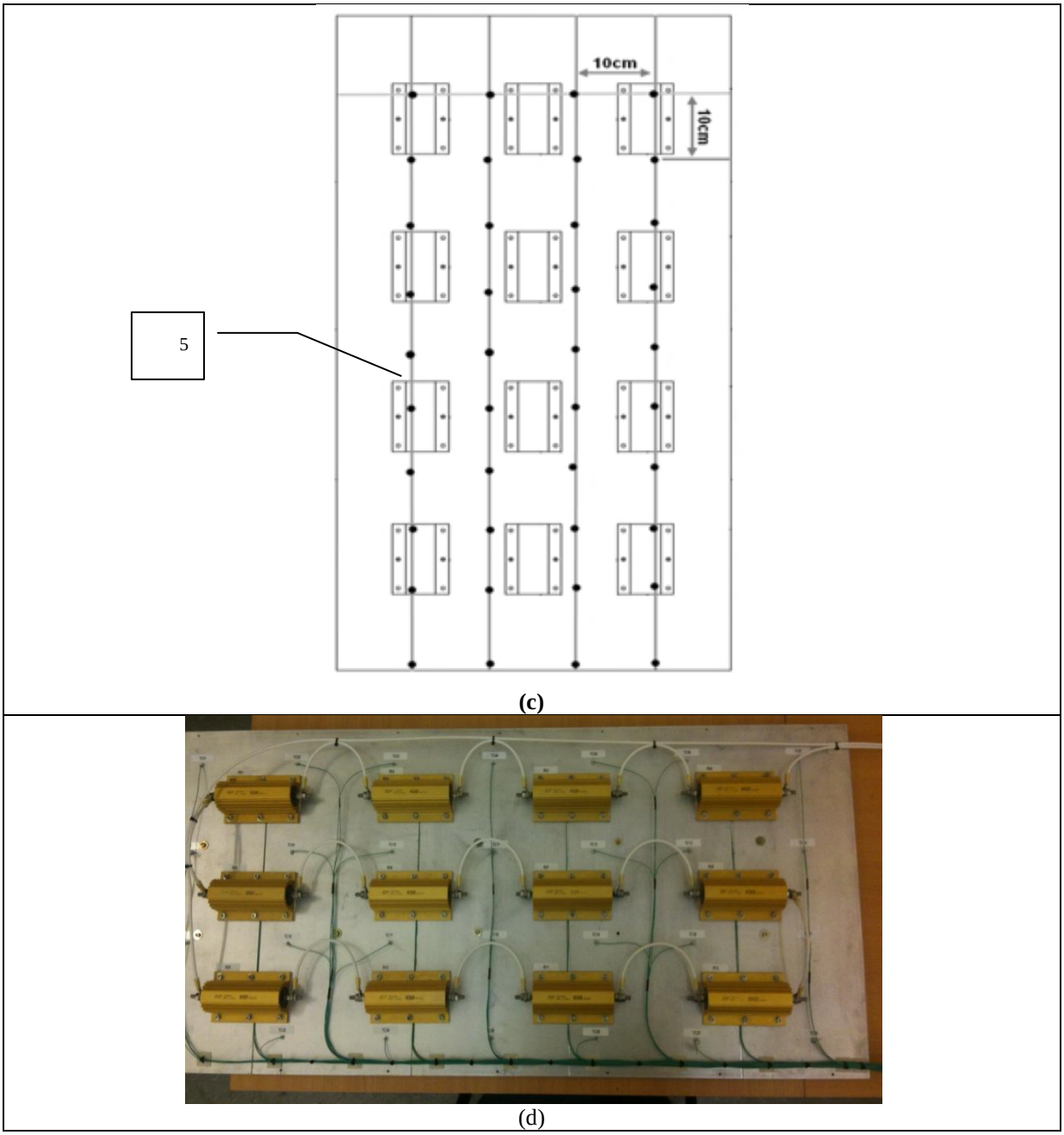

Figure 5 : **(a)** Front side of the experimental set-up, **(b)** Back side of the experimental set-up without insulating layer, **(c)** Thermocouple positions on the plate **(d)** picture of thermocouples and resistors on the plate. **1**: Aluminium plate **2**: Heating unit **3**: Insulating layer **4**: Plexiglas wall **5**: Thermocouple position.

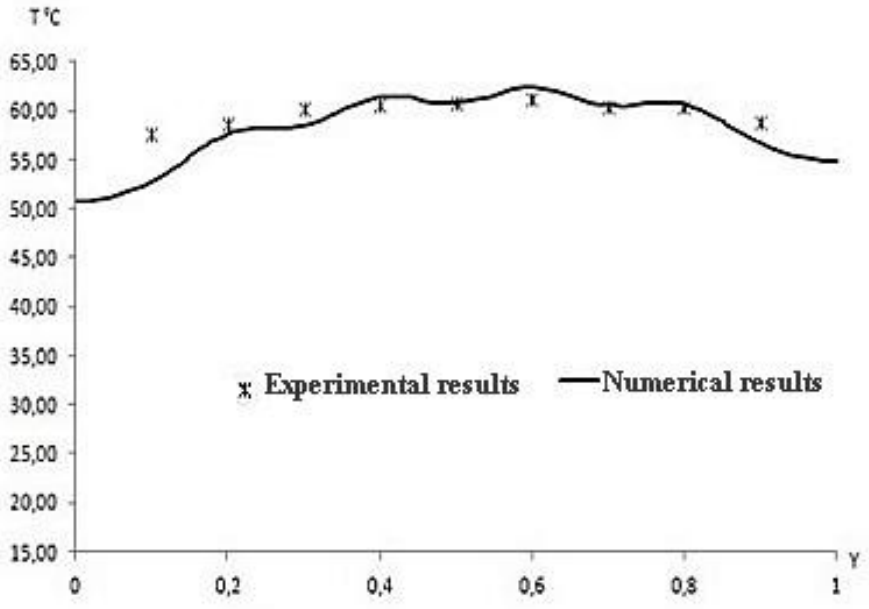

Figure 6 Comparisons of the numerical and experimental temperature profiles

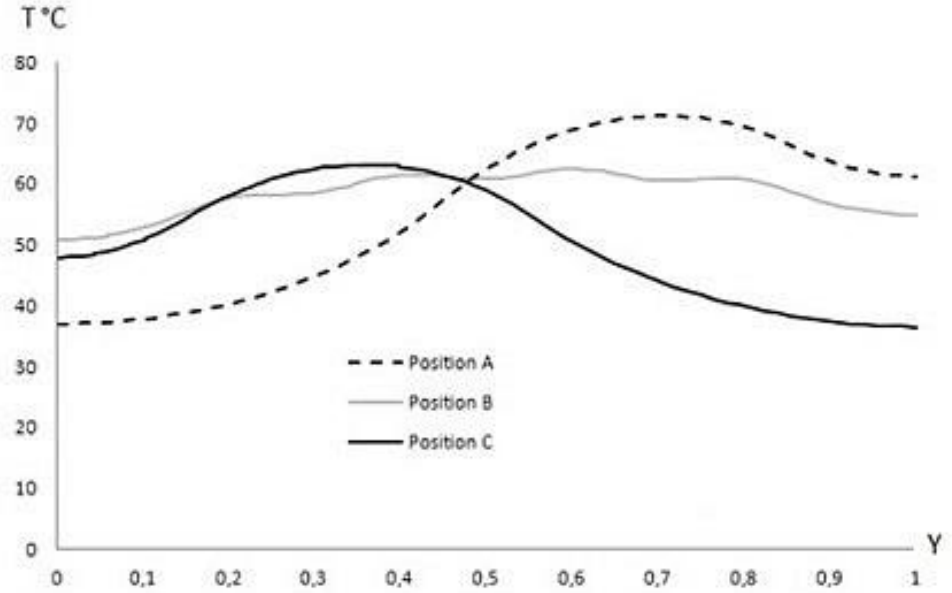

Figure 7 Comparison of temperature profiles along the plate for the three configurations.

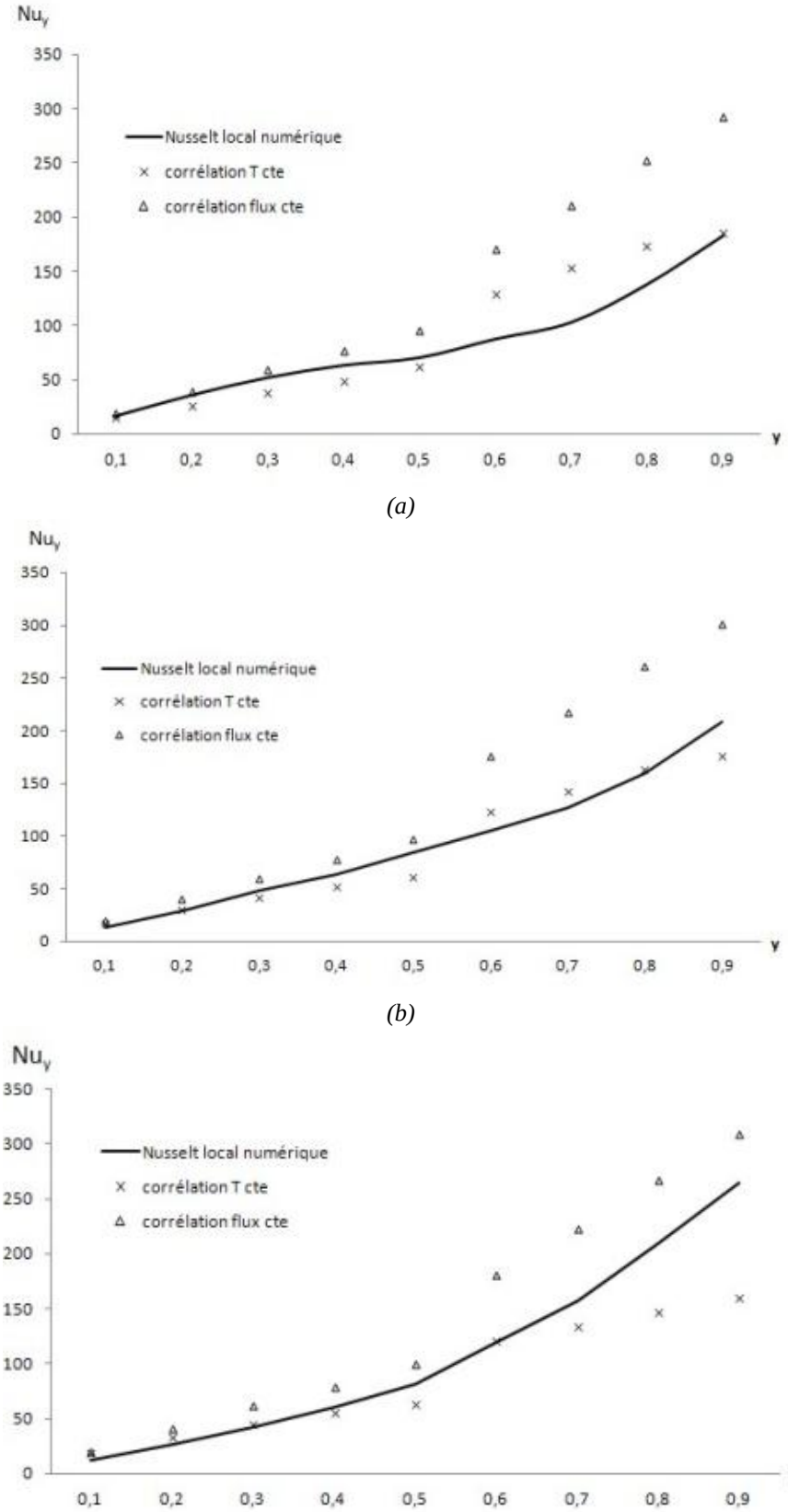

(a)

(b)

(c)

Figure 8 Comparison of the numerical local Nusselt number with the Mc Adams correlations ***(a)*** *Configuration A* ***(b)*** *Configuration B* ***(c)*** *Configuration C*

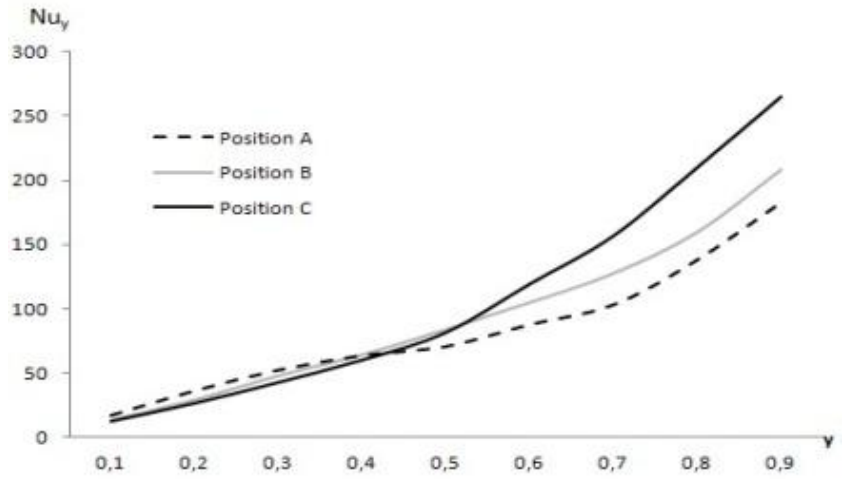

Figure 9 Comparison of the local Nusselt number profiles along the plate for the three configuration

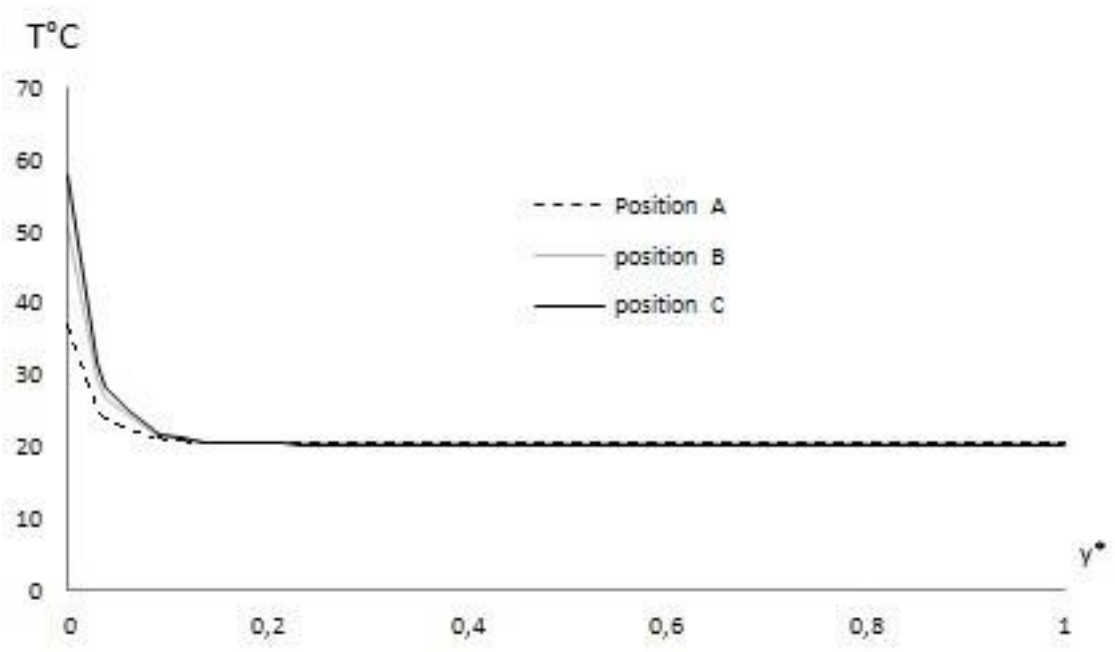

(a)

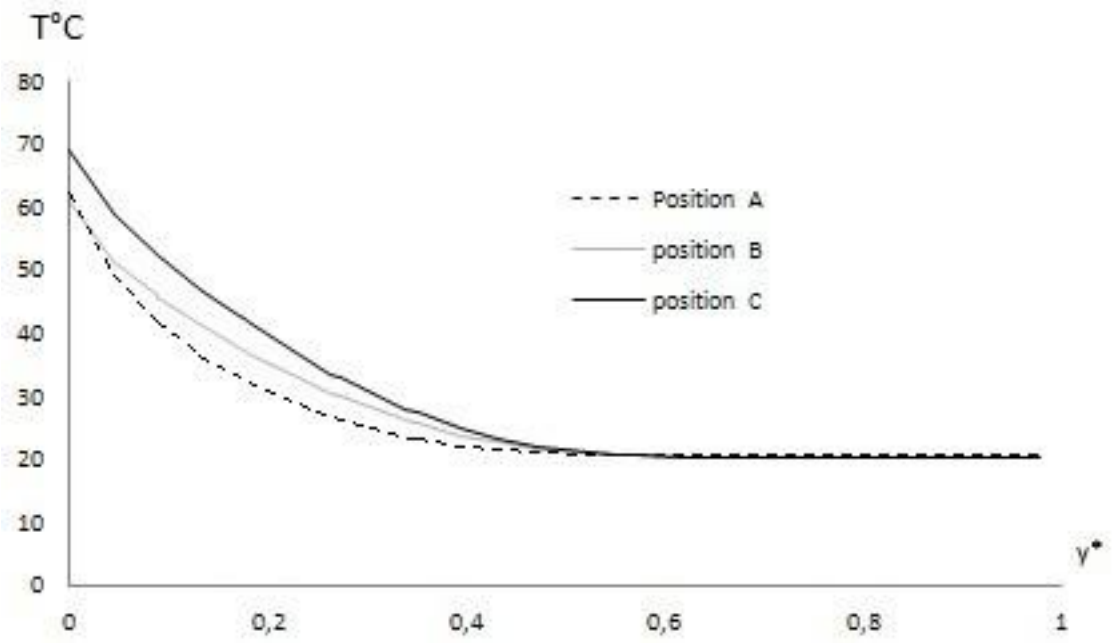

(b)

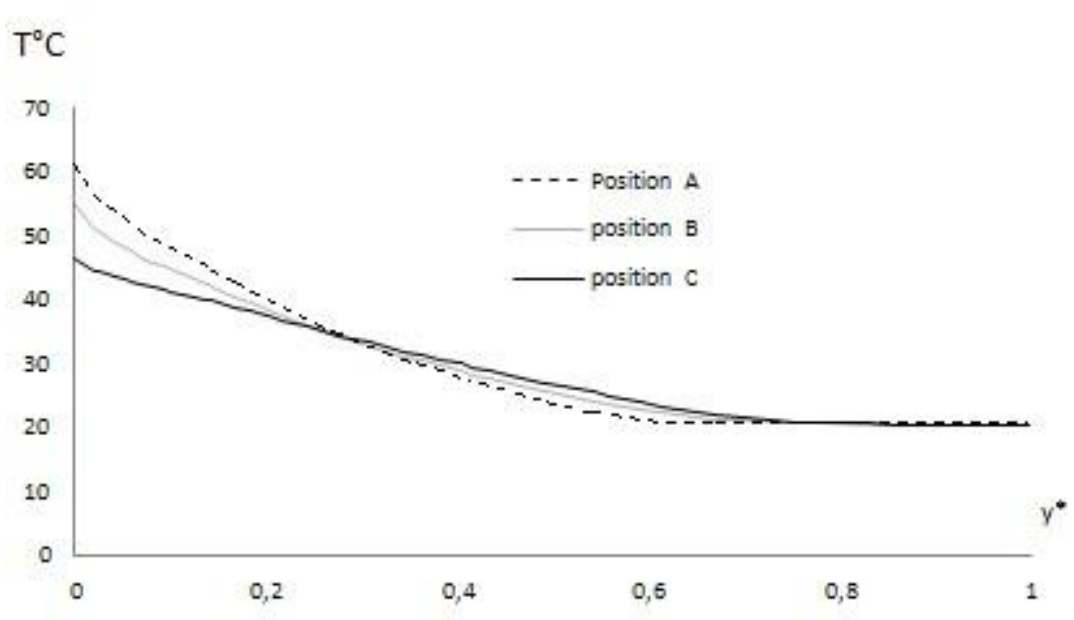

(c)

Figure 10 : Air temperature profiles for the three configurations at three positions ***(a)*** *y = 0.05m* ***(b)*** *y = 0.5m* ***(c)*** *y = 0.95m*

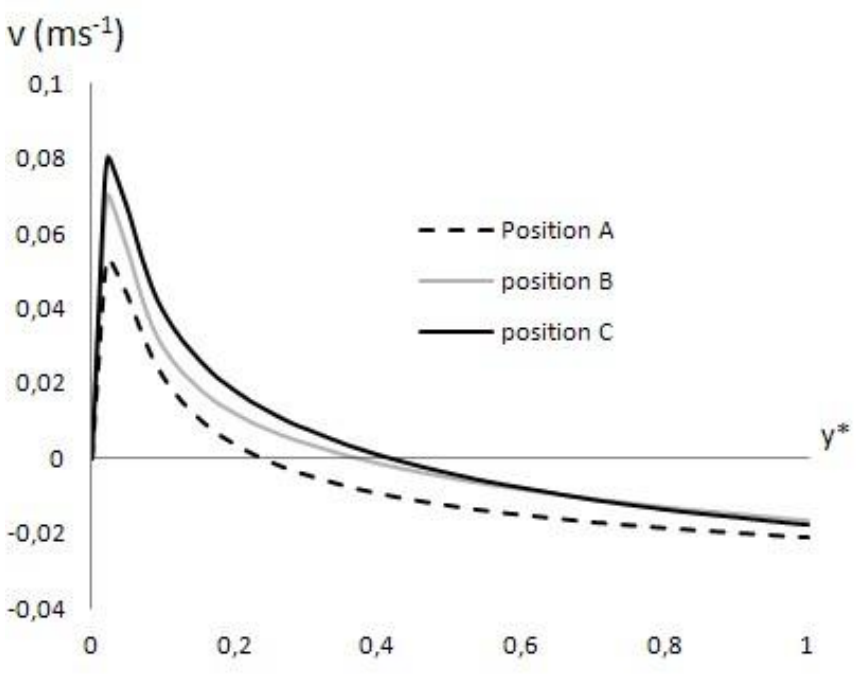
v (ms-1)
0,1
0,08
0,06
0,04
0,02
0
-0,02
-0,04
0
0,2
0,4
0,6
0,8
1
y*
Position A
position B
position C

(a)

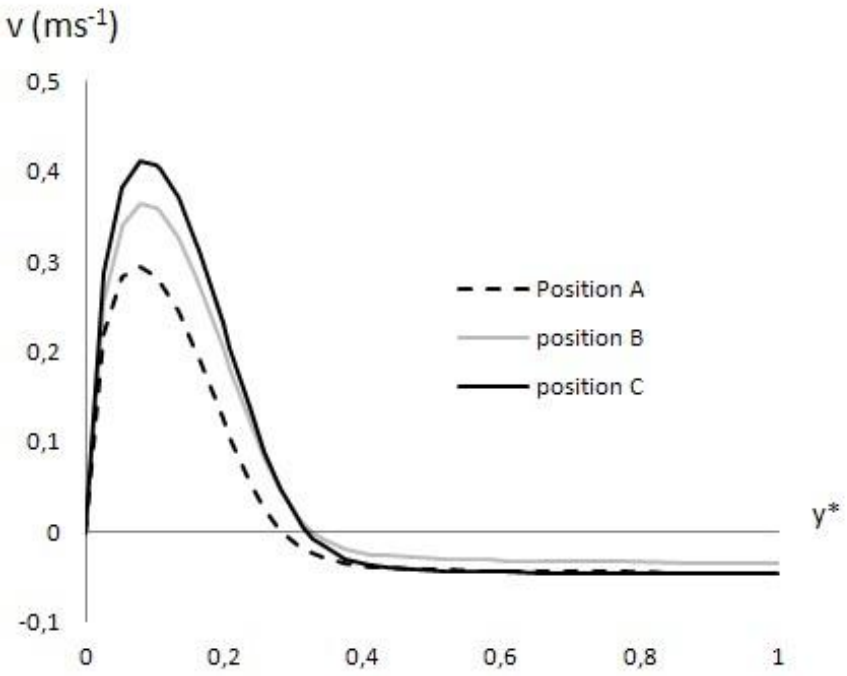
v (ms-1)
0,5
0,4
0,3
0,2
0,1
0
-0,1
0
0,2
0,4
0,6
0,8
1
y*
Position A
position B
position C

(b)

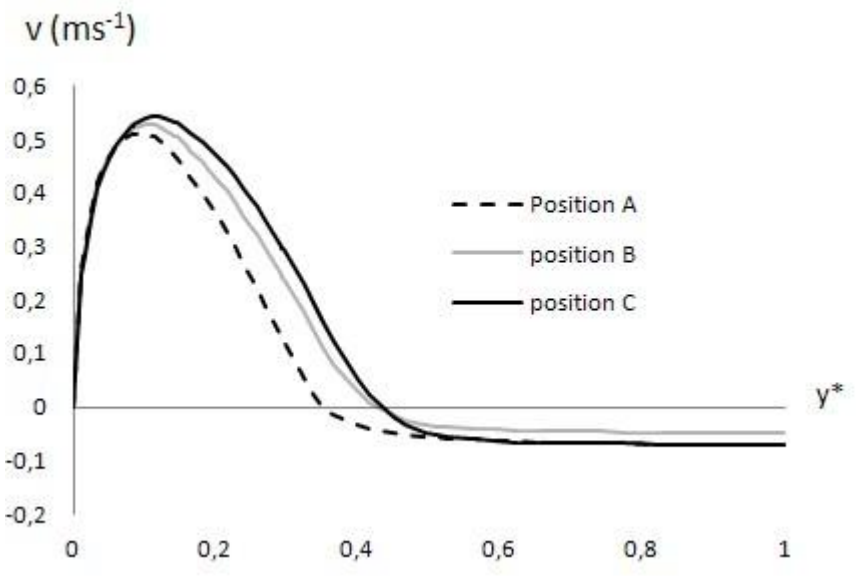

(c)

Figure 11 Air vertical velocity profiles for the three configurations at three levels ***(a)*** *y = 0.05m* ***(b)*** *y = 0.5m* ***(c)*** *y = 0.95m*

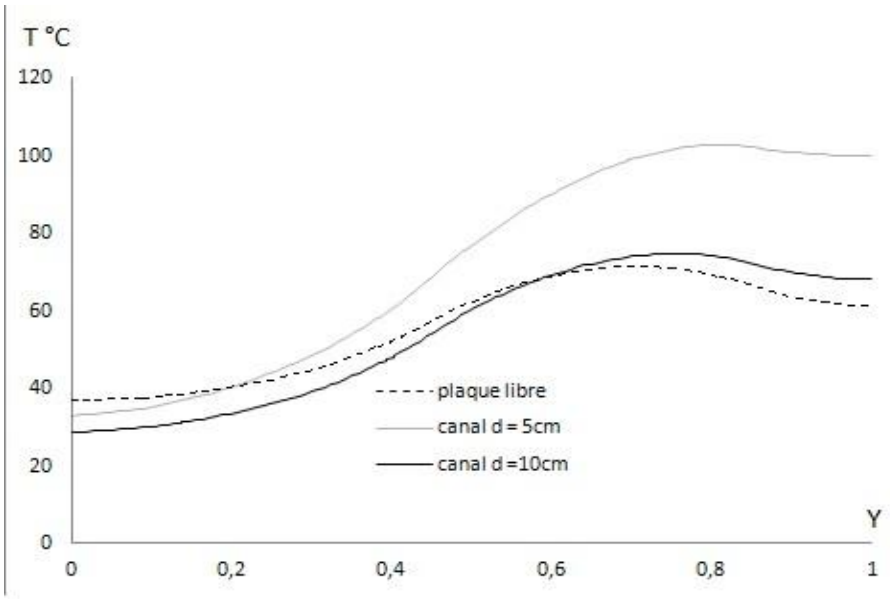

(a)

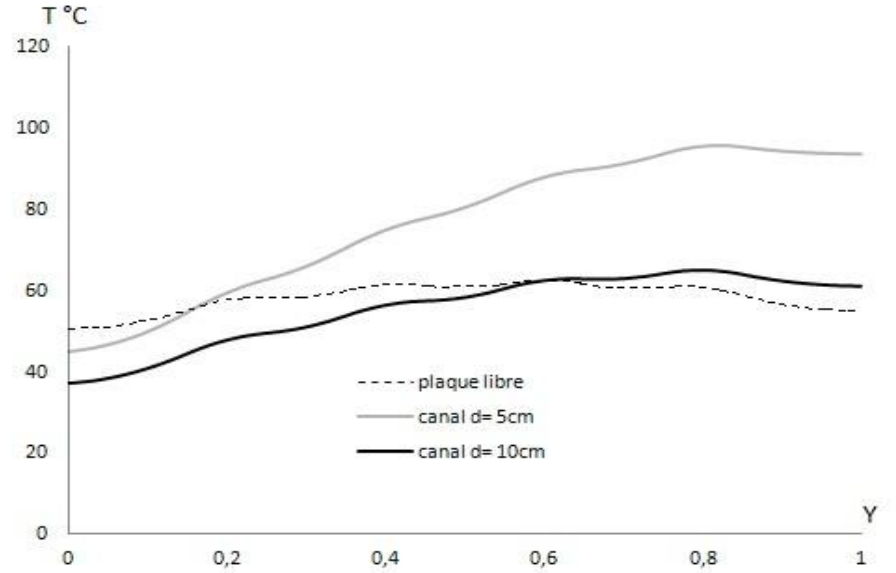

(b)

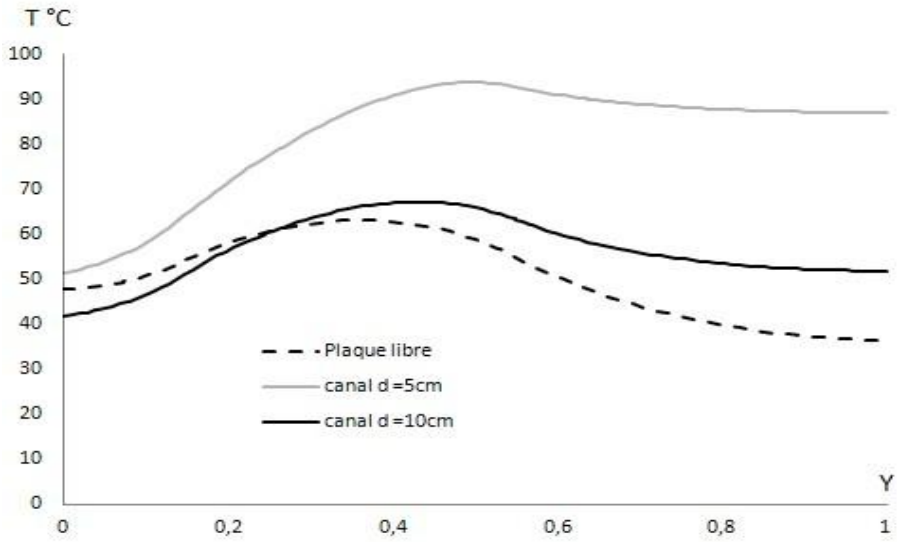

(c)

*F*igure 12 Comparison of the temperature profiles along the plate for channels of width d=5cm, d=10 cm and free vertical plate**(a)** Configuration A **(b)** Configuration B **(c)** Configuration C CHANGER LEGENDE

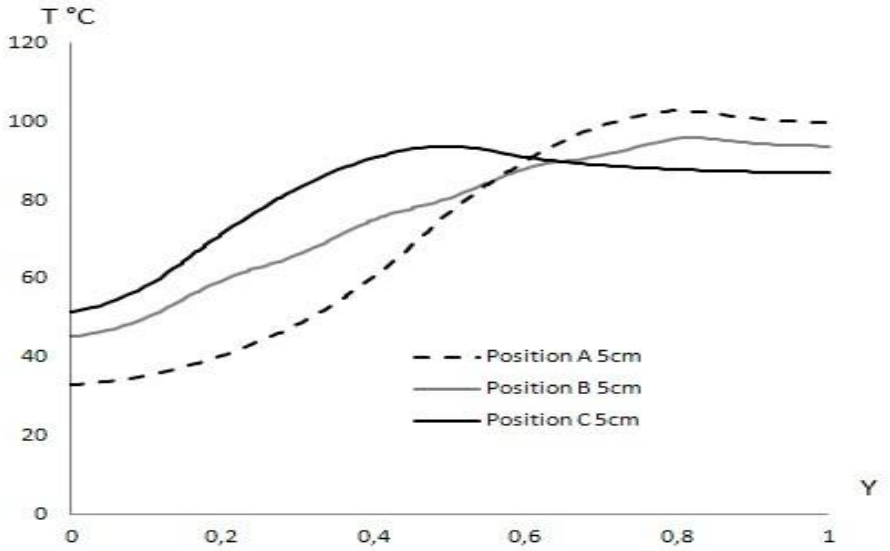

(a)

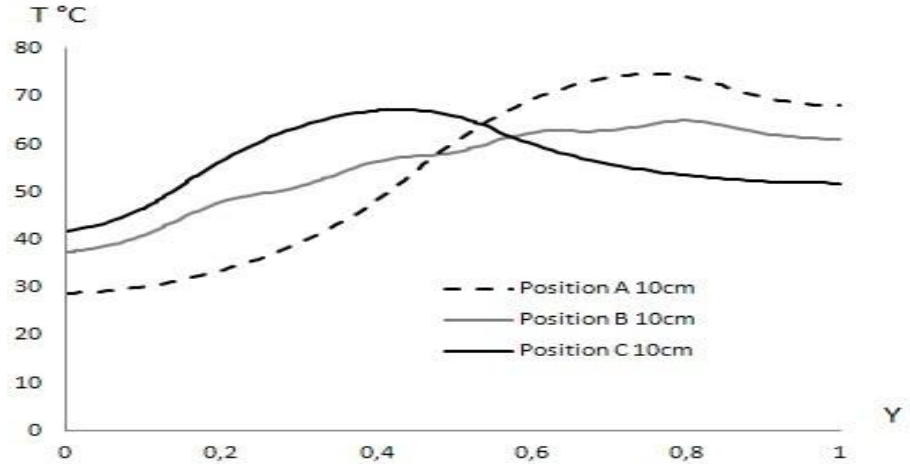

(b)

Figure 13 Temperature profiles along the plate for the three configurations ***(a)*** *Channel width d = 5cm* ***(b)*** *Channel width d = 5cm*

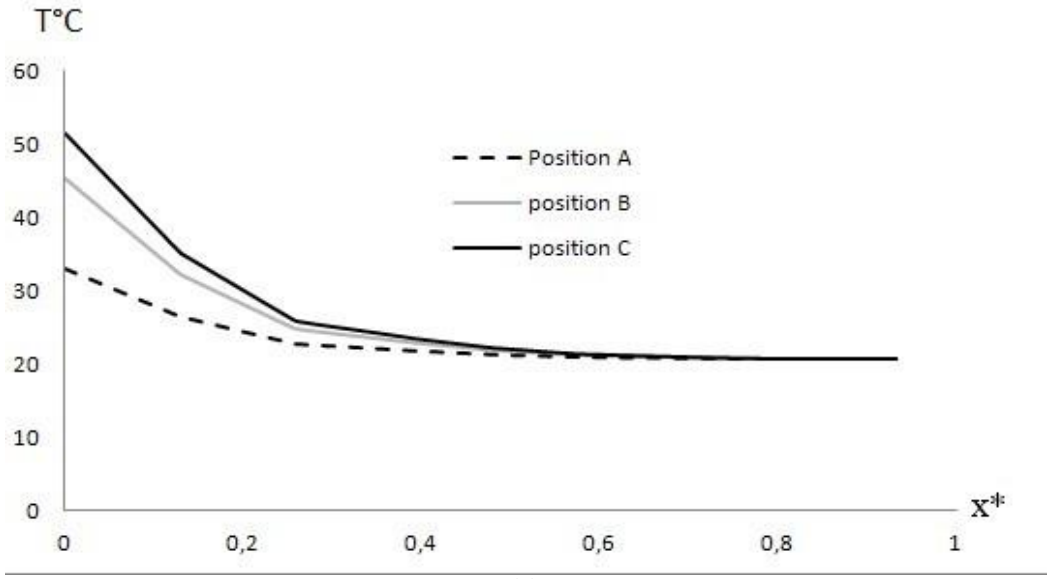

(a)

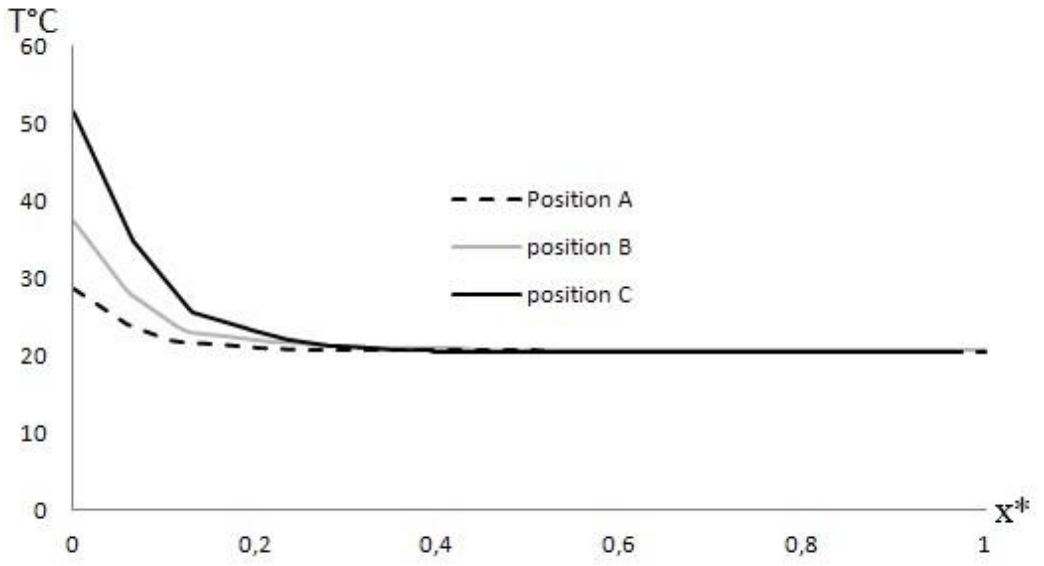
T°C
60
50
40
30
20
10
0
0
0,2
0,4
0,6
0,8
1
X*
Position A
position B
position C

(b)

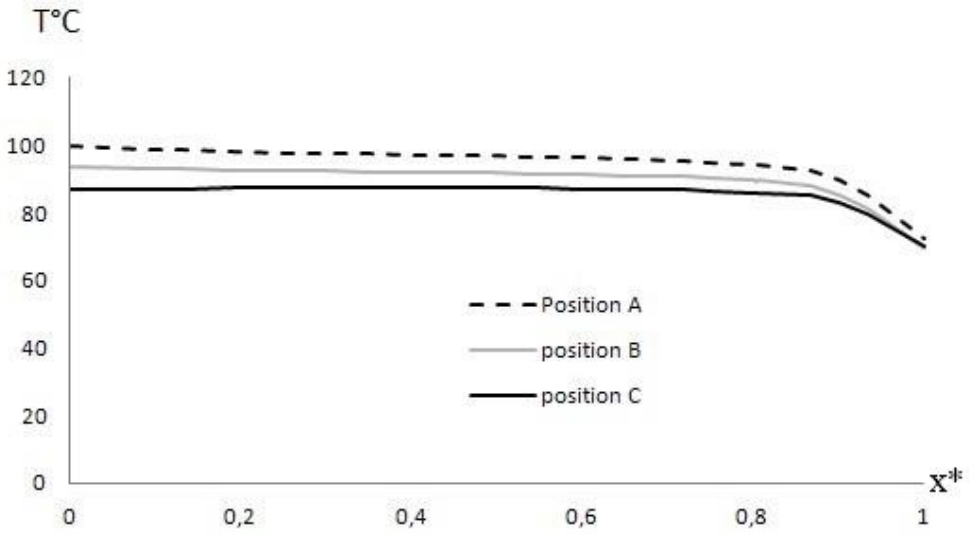
T°C
120
100
80
60
40
20
0
0
0,2
0,4
0,6
0,8
1
X*
Position A
position B
position C

(c)

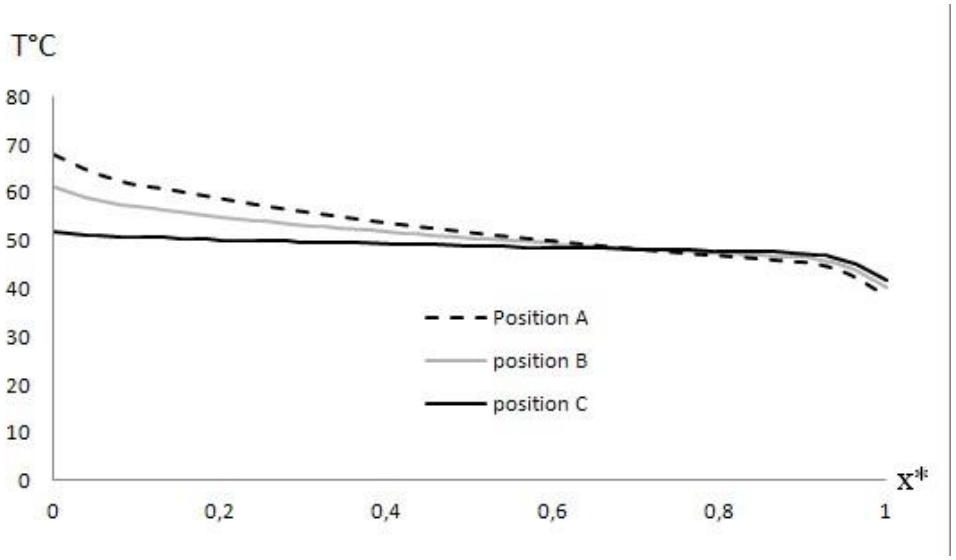

(d)

*Figure 14Air temperature profiles for the three configurations **(a)** At the entrance for channel width d = 5cm **(b)** At the entrance for channel width d = 10cm **(c)** At the exit for channel width d = 5cm **(d)** At the exit for channel width d = 10cm*

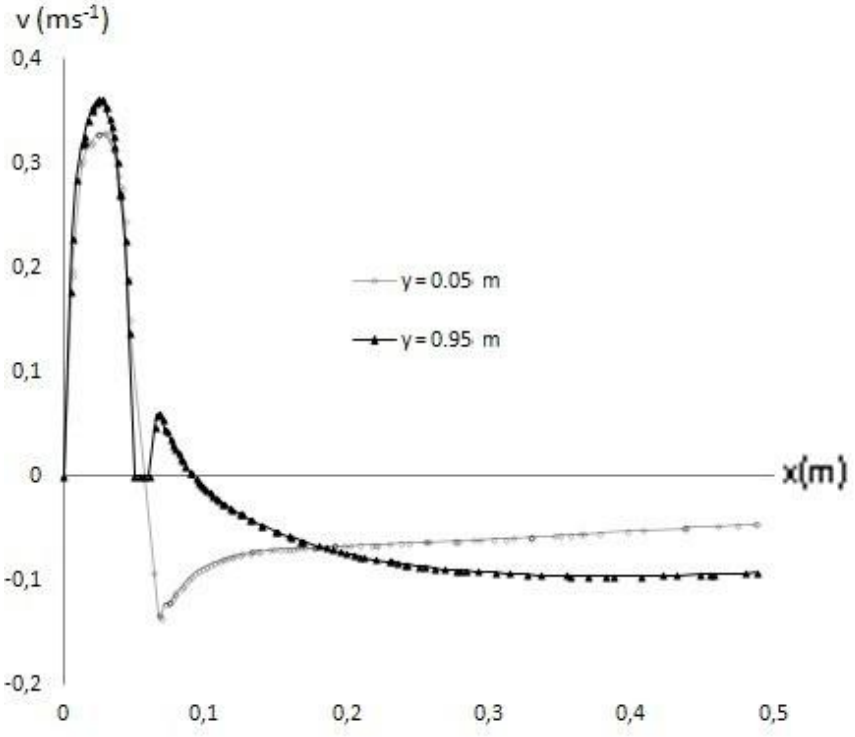

(a)

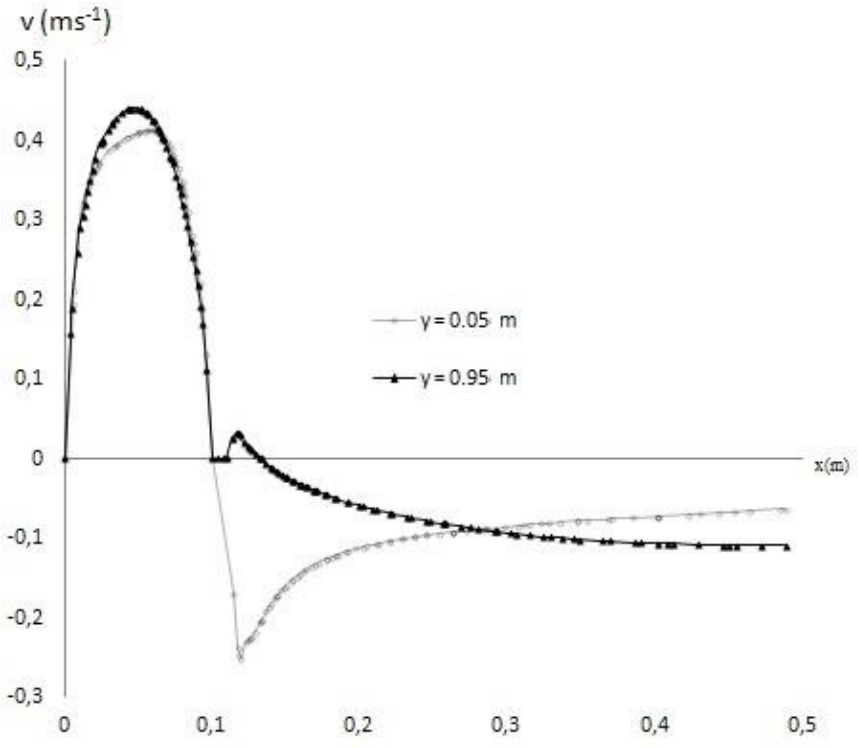

(b)

Figure 15 Air vertical velocity profiles at the entrance and the exit of channel for the configuration B ***(a)*** *Channel width d = 5cm* ***(b)*** *Channel width d = 10cm*